Int. J. Therm. Sci. (2001) 40, 165–172

S1290-0729(00)01205-9/FLA

Thermodynamic analysis of a heat-driven metal hydride cogeneration cycle

Thomas M. Ortiz [a], Eckhard A. Groll [a]*, Brad A. Meyer [b]

[a] *School of Mechanical Engineering, Purdue University, 1077 Ray W. Herrick Laboratories, West Lafayette, IN 47907-1077, USA*

[b] *Engineering Sciences and Applications Division, Los Alamos National Laboratory, P.O. Box 1663, MS G780, Los Alamos, NM 87545, USA*

(Received 17 December 1999, accepted 17 April 2000)

Abstract — A heat-driven metal hydride cogeneration cycle has been analyzed using classical first and second law analysis as well as finite-time thermodynamics. Second law analysis introduces important limitations on operating conditions not previously mentioned in the literature. The system being investigated is based on a cycle developed at Brookhaven National Laboratory. Predicted performance is compared to data from two other hydride power systems, HYCSOS (developed at Argonne National Laboratory) and a system developed by Bomin Solar, GmbH. Power generated per kg of hydridable alloy was highest for the present cycle (0.11 $kW{\cdot}kg^{-1}$) while useful heat or cold rates were highest for the HYCSOS cycle (0.30 $kW{\cdot}kg^{-1}$) and the system developed by Bomin Solar (0.30 $kW{\cdot}kg^{-1}$). Fuel-use efficiencies were highest for the present cycle (0.23), while second law efficiencies were highest for HYCSOS (0.60). Power and efficiency diagrams based on the finite temperature difference between the hydride bed and external heat transfer fluid are also presented. © 2001 Éditions scientifiques et médicales Elsevier SAS

cogeneration / thermodynamics / finite time / first law / second law / hydride / hydrogen / HYCSOS

Nomenclature

A	area	m^2
A, B, C	labels for hydride beds	
c	concentration of hydrogen (moles of H per mole of alloy)	
c_v	specific heat at constant volume	$kJ{\cdot}kg^{-1}{\cdot}K^{-1}$
c_p	specific heat at constant pressure	$kJ{\cdot}kg^{-1}{\cdot}K^{-1}$
D	argument of exponential function developed for readability	
h	enthalpy of hydrogen gas	$kJ{\cdot}kg^{-1}$
ΔH	heat of reaction for hydride formation	$kJ{\cdot}kg^{-1}$
i	irreversibility	$kJ{\cdot}kg^{-1}$
m	mass	kg
p	pressure	kPa
PMH	porous metallic hydride	
Q	heat transfer	kJ
r_{p-h}	power-to-heat ratio for hydride cogeneration cycle	
s	entropy of hydrogen gas	$kJ{\cdot}kg^{-1}{\cdot}K^{-1}$
ΔS	entropy of reaction for hydride formation	$kJ{\cdot}kg^{-1}{\cdot}K^{-1}$
ΔT	difference between reservoir and working fluid temperatures	K
t	time	s
T	temperature	K
U	overall heat transfer coefficient	$kW{\cdot}m^{-2}{\cdot}K^{-1}$
u	internal energy of hydrogen gas	$kJ{\cdot}kg^{-1}$
W	work output	kJ

Greek symbols

α	stoichiometric coefficient of hydrogen gas	
γ	ratio of ideal gas specific heats	
ε_f	fuel-use efficiency	
ε_2	second law efficiency	
σ	entropy generation	$kJ{\cdot}kg^{-1}{\cdot}K^{-1}$

Subscripts

0	start of desorption process, end of isosteric heating process
1	end of desorption process, inlet of heat exchanger
2	outlet of heat exchanger
3	turbine inlet

* Correspondence and reprints.
E-mail addresses: ortizt@ecn.purdue.edu (T.M. Ortiz), groll@ecn.purdue.edu (E.A. Groll).

4	turbine outlet, inlet of heat exchanger
5	outlet of heat exchanger
6	start of absorption process
7	end of absorption process, start of isosteric heating process
ambient	environmental conditions
cycle	refers to entire cycle
H	hydrogen
m	unhydrided metal or alloy
hyd	hydrided metal or alloy
source	external high temperature heat source
space	condition of heated or cooled space

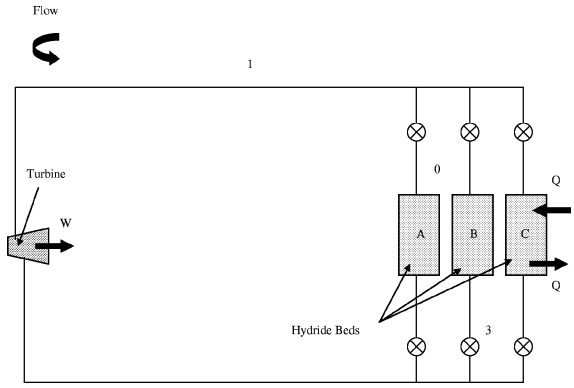

Figure 1. Simplified flow diagram for HYCSOS system.

1. INTRODUCTION

Metal hydride energy utilization systems have been studied extensively since the mid-1970s [1, 2]. Cogeneration systems were investigated at Brookhaven and Argonne National Laboratories in the US (the latter under the auspices of the HYCSOS project) and more recently by Bomin Solar, GmbH in Germany. However, recent interest has focused on heat pump and refrigeration systems. The hydride power and cogeneration system literature appears to be confined to first-law analyses and performance estimates are made with respect to an ideal (Carnot) cycle. It is the aim of this paper to perform classical first and second law analyses of a hydride cogeneration cycle with hydrogen gas as the working fluid and then to calculate power and heat rates as well as first and second law efficiencies as functions of finite temperature differences across which the heat transfers will occur.

Terry and Schoeppel [3] patented a design for heat-driven metal hydride cogeneration systems at Brookhaven National Laboratory. Their application was a bottoming cycle using waste heat from a conventional nuclear or fossil-fuel power plant. A similar system was analyzed on a first law basis by Powell et al. [4]. The HYCSOS and Bomin Solar systems used solar collectors to provide the driving heat for the cycle. The HYCSOS system, as presented by Gruen et al. [5], was proposed as an off-peak energy storage system in conjunction with conventional power sources and is very similar to the Brookhaven cycle. The Bomin Solar system was designed for use by small rural communities without access to a power grid [6].

In HYCSOS and the present cycle hydrogen gas is a working fluid which traverses what is essentially an air-standard Brayton cycle. The principal difference between the present cycle and HYCSOS is that the latter does not make use of heat exchangers for precooling the expansion

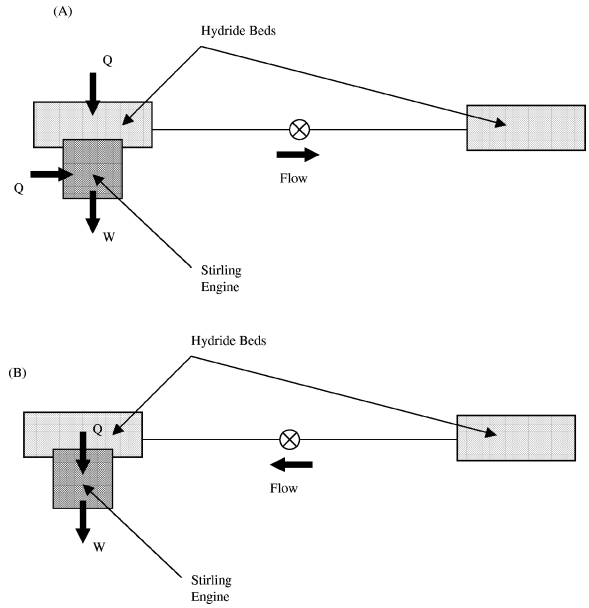

Figure 2. Flow diagrams for Bomin Solar system: (A) daytime operation, (B) nighttime operation.

gas or internal regeneration (see *figure 1*). The system of Powell et al. [4] does include precooling as well as a heat exchanger to preheat the turbine exhaust before absorption. In HYCSOS process heat is generated by operating the absorption stage at a higher temperature than the ambient [5].

The Bomin Solar system utilizes a Stirling engine to generate electricity. During the daytime, insolation provides driving heat for the Stirling engine as well as heat to desorb gas from a hydride bed (see *figure 2*). The gas is reabsorbed into a second bed, which becomes a store of thermal energy. Process heat may also be removed at this stage. At night or during periods of

low insolation this thermal store is desorbed by opening the valve between it and the other (empty) bed. The corresponding heat of absorption drives the Stirling engine under these conditions, providing a continuous power source.

Ikeda et al. [7] presented a power cycle in which the heat generated by absorption of hydrogen by a metal is used to boil water and thereby drive a steam turbine. In this fashion, the hydride beds are analogous to the fuel rods in a nuclear power plant. Process heat could be generated by bleeding steam from the turbine exhaust. This system could be represented by the Rankine cycle with the hydride integral to the boiler.

Metal and hydrogen can bond in two ways. The elements can form a solution or they can form a stable stoichiometric compound (hydride). The formation of hydride is highly exothermic and nearly reversible [8]. By adding heat to a hydride bed the gas can be desorbed at high pressures. This chemical pumping action alleviates the need for a mechanical compressor.

The generic hydride formation reaction is shown in equation (1):

$$\mathrm{M(solid)} + \frac{\alpha}{2}\mathrm{H_2(gas)} \Leftrightarrow \mathrm{MH_\alpha(solid)} + \Delta H \quad (1)$$

The relationship between pressure, temperature and the heat of hydride formation is given by the Van't Hoff equation

$$\ln\left(\frac{P}{P_{\mathrm{ref}}}\right) = \frac{\Delta H}{RT} - \frac{\Delta S}{R} \quad (2)$$

where ΔH is the enthalpy, ΔS the entropy of hydride formation and P_{ref} is a reference pressure taken to be 1 bar. The thermodynamic properties are approximately independent of temperature over a wide range [9] and the formation of hydride from metal and hydrogen occurs at nearly constant pressure. This constant pressure region of the metal–hydrogen phase diagram is referred to as the plateau. In actuality, the plateau is not entirely flat. However, operating the present cycle in the plateau region of *figure 3* will result in a nearly constant pressure ratio across the turbine. A representative isotherm of the $LaNi_5$–H system is shown in *figure 3*. $LaNi_5$ has been extensively studied and used as a hydridable alloy [10]. Advantages of $LaNi_5$ include its small plateau slope and favorable pressure–temperature characteristics.

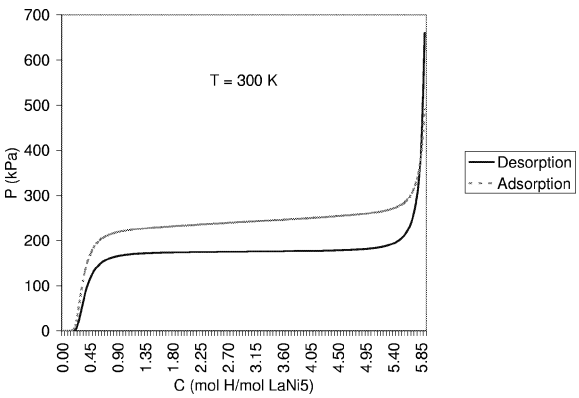

Figure 3. Desorption and adsorption isotherms for the $LaNi_5$–H system at 300 K.

2. PRESENT CYCLE

Figure 4 shows a flow diagram of a simple hydride cogeneration cycle. It is based on those of Terry and Schoeppel [3] and Powell et al. [4] without multiple expansion stages or reheat stages, respectively. The cycle produces both electrical work (process 3–4) and either useful heat (process 1–2) or useful cold (process 4–5) and is driven by heat input to the hydride beds (marked A, B and C). The cycle communicates with three thermal reservoirs, which are at temperatures T_{source}, T_{ambient} and T_{space}. These are the temperatures of the driving heat source, the environment and the heated or cooled space, respectively. *Table I* lists the processes which occur during the course of one complete cycle, *figure 4* is a flow diagram for the present cycle and *figure 5* shows each state point of the present cycle in a pressure–composition–temperature (PCT) diagram.

A fixed quantity of hydrogen modeled as an ideal gas is the working fluid. This hydrogen starts out in solid hydride form in one bed at state 0. It is at T_{source} and pressure as calculated by equation (2). Its composition is such as to place it at the rightmost boundary of the plateau region (refer to *figure 1*). Hydrogen gas is now

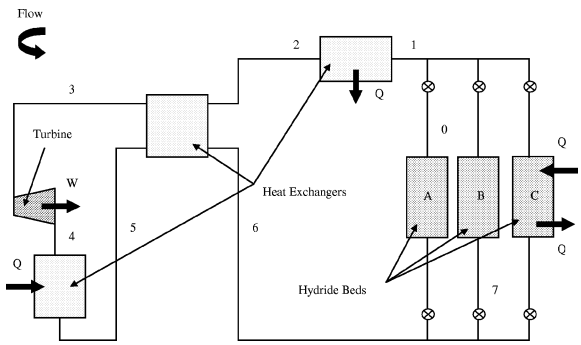

Figure 4. Flow diagram for hydride cogeneration cycle.

TABLE I
Hydride cogeneration cycle processes.

Process	Description
0–1	isothermal desorption
1–2	isobaric cooling (space heating)
2–3	isobaric (regenerative) cooling
3–4	isentropic expansion (power output)
4–5	isobaric heating (space cooling)
5–6	isobaric (regenerative) heating
6–7	isothermal absorption
7–0	isosteric heating
1–6	isosteric cooling

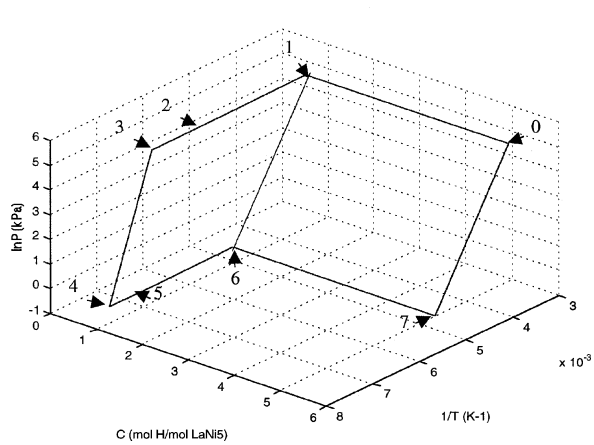

Figure 5. PCT surface for hydride cogeneration cycle.

driven from the bed by the addition of heat from the high temperature source until the bed has crossed to the leftmost (low concentration) boundary of the plateau.

The liberated gas is now cooled, first by rejecting heat to the environment (or heated space) — which brings it to state 2 — and then by passing through the regenerative heat exchanger where it is cooled below ambient temperature before being expanded through the turbine to state 4. The expansion process is assumed to be isentropic and cools the gas below the temperature of the cooled space (or environment). The principal difference between the systems of Terry and Schoeppel and of Powell et al. is that the former utilizes a heat exchanger to precool the expansion gas while the latter assumes a long transmission line over which the gas loses heat to the environment.

Now, at low pressure and low temperature, the gas accepts heat from the cooled space and passes through the regenerator where it is heated by the other gas stream to the environmental or intermediate temperature (state 6). A second bed is at low concentration and at ambient temperature. Its pressure under these conditions is lower than the turbine outlet pressure. This pressure gradient drives the absorption of gas into the bed; the heat of absorption is rejected to ambient in order to maintain the bed at constant temperature and pressure.

The final stage of the cycle involves isolation of the absorbed and desorbed beds whereupon the newly charged bed is heated from T_{ambient} to T_{source} (7–0) and the depleted bed is cooled from T_{source} to T_{ambient} (1–6). Meanwhile, the third (charged) bed is desorbed at T_{source}. The cycle is now complete. This alternating cycle of desorption, absorption and heating experienced by each of the beds allows for continuous (quasi-steady) operation of the system.

The following analysis illustrates the operation of this cycle in cooling mode. The heating mode is analogous, with T_{space} in that case referring to the temperature of the reservoir communicating with heat exchanger 1–2 and T_{ambient} referring to the temperature of the reservoir communicating with heat exchanger 4–5. All other processes are identical.

3. FIRST AND SECOND LAW ANALYSIS

Each cycle process is analyzed using classical thermodynamics assuming constant properties at each state point over time. Thus, the total mass of hydrogen defined by the width of the plateau (in moles of H_2) passes through each state of the cycle in succession. The energy balances for each process are given below starting with the isothermal desorption (0–1):

$$Q_{0-1} = m_{\text{H}}(\Delta H_{\text{des}} + h_{0,1} - u_{0,1}) \tag{3}$$

$$Q_{1-2} = m_{\text{H}}(h_2 - h_1) \tag{4}$$

$$W_{3-4} = m_{\text{H}}(h_3 - h_4) \tag{5}$$

$$Q_{4-5} = m_{\text{H}}(h_5 - h_4) \tag{6}$$

$$Q_{6-7} = m_{\text{H}}(\Delta H_{\text{ads}} - h_{6,7} + u_{6,7}) \tag{7}$$

$$Q_{7-0} = m_{\text{hyd}} c_{\text{p,hyd}}(T_0 - T_7) \tag{8}$$

$$Q_{1-6} = m_{\text{m}} c_{\text{p,m}}(T_6 - T_1) + m_{\text{H,min}}(u_6 - u_1) \tag{9}$$

The entropy balances for each process are now given:

$$\sigma_{0-1} = m_{\text{H}}(\Delta S_{\text{des}}) - \frac{Q_{0-1}}{T_{\text{source}}} \tag{10}$$

$$\sigma_{1-2} = m_{\text{H}}(s_2 - s_1) - \frac{Q_{1-2}}{T_{\text{ambient}}} \tag{11}$$

$$\sigma_{3-4} = m_{\text{H}}(s_4 - s_3) \tag{12}$$

$$\sigma_{4-5} = m_{\text{H}}(s_5 - s_4) - \frac{Q_{4-5}}{T_{\text{space}}} \tag{13}$$

$$\sigma_{6-7} = m_{\mathrm{H}}(\Delta S_{\mathrm{ads}}) - \frac{Q_{6-7}}{T_{\mathrm{ambient}}} \tag{14}$$

$$\sigma_{7-0} = m_{\mathrm{hyd}} c_{\mathrm{p,hyd}} \ln\left(\frac{T_0}{T_7}\right) - \frac{Q_{7-0}}{T_{\mathrm{source}}} \tag{15}$$

$$\sigma_{1-6} = m_{\mathrm{m}} c_{\mathrm{p,m}} \ln\left(\frac{T_6}{T_1}\right) + m_{\mathrm{H,min}}(s_6 - s_1) - \frac{Q_{1-6}}{T_{\mathrm{ambient}}} \tag{16}$$

Irreversibilities are calculated using equations of the form

$$i_{i-j} = \sigma_{i-j} T_{\mathrm{ambient}} \tag{17}$$

The temperatures at states 6 and 7 are constrained by the regenerator heat balance

$$h_2 - h_3 = h_6 - h_5 \tag{18}$$

The following three performance parameters [11] will be used in the discussion which is to follow. The fuel use efficiency for the cycle is given by

$$\varepsilon_{\mathrm{f}} = \frac{|W_{3-4}| + |Q_{4-5}|}{|Q_{7-0}| + |Q_{0-1}|} \tag{19}$$

the power-to-heat (or cooling) ratio is given by

$$r_{\mathrm{p-h}} = \frac{|W_{3-4}|}{|Q_{4-5}|} \tag{20}$$

and the second law efficiency of the cycle is given by

$$\varepsilon_2 = \frac{|W_{3-4}| + |Q_{4-5}(1 - T_{\mathrm{ambient}}/T_{\mathrm{space}})|}{|(Q_{7-0} + Q_{0-1})(1 - T_{\mathrm{ambient}}/T_{\mathrm{source}})|} \tag{21}$$

Note that equations (3), (7), (10) and (14) may be used together to determine the maximum possible absorption reservoir temperature and the minimum permissible desorption reservoir temperature by constraining the respective entropy generation terms to be non-negative. This is an important limitation on operating conditions as it places bounds on the heat source and ambient temperatures the cycle may communicate with.

4. FINITE-TIME THERMODYNAMIC ANALYSIS

Classical thermodynamics predicts reversible cycles to have the best performance in terms of energetic and exergetic efficiency. A finite-time thermodynamic approach is now used in order to estimate the rates of useful work and heat generated in the cogeneration cycle. Finite-time thermodynamics has been used to model real cycle performance since 1975 [14]. Any real cycle that generates power or heat transfer at a finite rate must be irreversible since the cycle must communicate with reservoirs across a finite temperature difference. Reversible processes occur infinitely slowly and, therefore, generate no power or heat rate.

The time required to realize a heat transfer of magnitude Q is given by

$$t = \frac{Q}{UA\Delta T} \tag{22}$$

where U is the overall heat transfer coefficient between the heat transfer surface and the reservoir and ΔT is the magnitude of the finite temperature difference between them. The operation of the cycle is quasi-steady; all processes except for the isosteric heating and cooling occur simultaneously [12]. The absorption and desorption processes determine the flow rate of gas in the system. Times for absorption and desorption are calculated as

$$t_{6-7} = \mathrm{abs}\left(\frac{m_{\mathrm{H}}(\Delta H_{\mathrm{ads}} - h_{6,7} + u_{6,7})}{(UA)_{6-7}(T_{6,7} - T_{\mathrm{ambient}})}\right) \tag{23}$$

and

$$t_{0-1} = \mathrm{abs}\left(\frac{m_{\mathrm{H}}(\Delta H_{\mathrm{des}} + h_{0,1} - u_{0,1})}{(UA)_{0-1}(T_{\mathrm{source}} - T_{0-1})}\right) \tag{24}$$

respectively. The isosteric heating and cooling times are calculated as

$$t_{7-0} = \mathrm{abs}\left(\frac{m_{\mathrm{hyd}} c_{\mathrm{p,hyd}} \ln((T_{\mathrm{source}} - T_7)/(T_{\mathrm{source}} - T_0))}{(UA)_{7-0}}\right) \tag{25}$$

and

$$t_{1-6} = \mathrm{abs}\left(\left(m_{\mathrm{m}} c_{\mathrm{p,m}} + m_{\mathrm{H,min}} c_{\mathrm{v,H}}(T_{\mathrm{avg}})\right) \cdot \frac{\ln((T_6 - T_{\mathrm{ambient}})/(T_1 - T_{\mathrm{ambient}}))}{(UA)_{1-6}}\right) \tag{26}$$

respectively. The cycle time is the sum of the largest of the absorption and desorption processes and the largest of the isosteric heating and cooling processes:

$$t_{\mathrm{cycle}} = \max(t_{6-7}, t_{0-1}) + \max(t_{7-0}, t_{1-6}) \tag{27}$$

Gruen et al. [13] note that the cycle time is "determined primarily by the time needed for absorption which in turn is strongly dependent on the heat transfer from the

cooling fluid to the absorbing metal powder". The power and useful cold generated by the cycle then become

$$\dot{W} = \frac{W_{3-4}}{t_{\text{cycle}}} \tag{28}$$

and

$$\dot{Q} = \frac{Q_{4-5}}{t_{\text{cycle}}} \tag{29}$$

respectively.

5. POWER AND EFFICIENCY DIAGRAMS

The effect of design parameters on cycle performance can be determined by expressing equations (28) and (29) (as well as the equivalent of equation (29) for heating mode operation) in terms of ΔT, which was considered to be the same for both the absorption and desorption processes in order to have an unambiguous expression for the cycle time. The transformed equations become

$$\dot{W}_{3-4} = \frac{UAc_{\text{ph}}\Delta T(T_{\text{space}} - \Delta T)(1 - \exp(D))}{R(T_{\text{ambient}} + \Delta T) - \Delta H_{\text{ads}}} \tag{30}$$

$$\dot{Q}_{4-5} = \frac{UAc_{\text{ph}}\Delta T(T_{\text{space}} - (T_{\text{space}} - \Delta T)\exp(D))}{R(T_{\text{ambient}} + \Delta T) - \Delta H_{\text{ads}}} \tag{31}$$

and

$$\dot{Q}_{1-2} = \frac{UAc_{\text{ph}}\Delta T(T_{\text{space}} - T_{\text{source}} + \Delta T)}{R(T_{\text{ambient}} + \Delta T) - \Delta H_{\text{ads}}} \tag{32}$$

with

$$D = \frac{\Delta H_{\text{ads}}}{R}\,\frac{\gamma - 1}{\gamma}\,\frac{(T_{\text{source}} - 2\Delta T - T_{\text{ambient}})}{(T_{\text{source}} - \Delta T)(T_{\text{ambient}} + \Delta T)} \tag{33}$$

introduced for increased readability. Note that the ideal gas specific heat has been assumed constant in order to simplify this part of the analysis. With the additional transformation of equations (3)–(6) and (8) to

$$Q_{0-1} = m_{\text{h}}\big(\Delta H_{\text{des}} + R(T_{\text{source}} - \Delta T)\big) \tag{34}$$

$$Q_{1-2} = m_{\text{h}}c_{\text{ph}}(T_{\text{space}} - T_{\text{source}} + \Delta T) \tag{35}$$

$$W_{3-4} = m_{\text{h}}c_{\text{ph}}(T_{\text{space}} - \Delta T)\big(1 - \exp(D)\big) \tag{36}$$

$$Q_{4-5} = m_{\text{h}}c_{\text{ph}}\big(T_{\text{space}} - (T_{\text{space}} - \Delta T)\exp(D)\big) \tag{37}$$

and

$$Q_{7-0} = m_{\text{hyd}}c_{\text{p,hyd}}(T_{\text{source}} - 2\Delta T - T_{\text{ambient}}) \tag{38}$$

equations (19) and (21) can then be recast in terms of ΔT or, equivalently, desorption temperature since the two differ only by a constant. *Figures 6* and *7* illustrate the effects of desorption temperature (which implies the effect of cycle time at constant UA) on power, heat or cold rate and both fuel-use and second law efficiencies. Relevant system parameters used to construct *figures 6* and *7* are listed in *table II*.

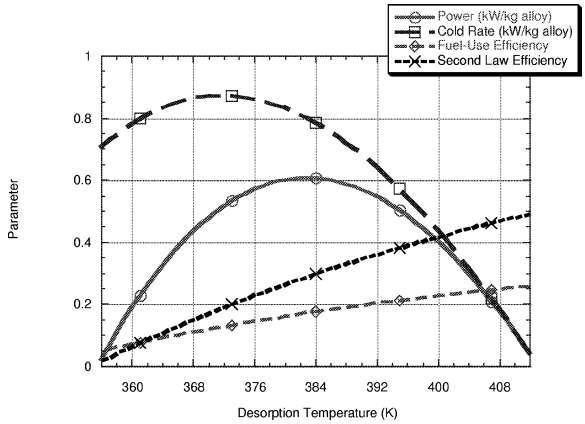

Figure 6. Cooling mode performance as a function of desorption temperature.

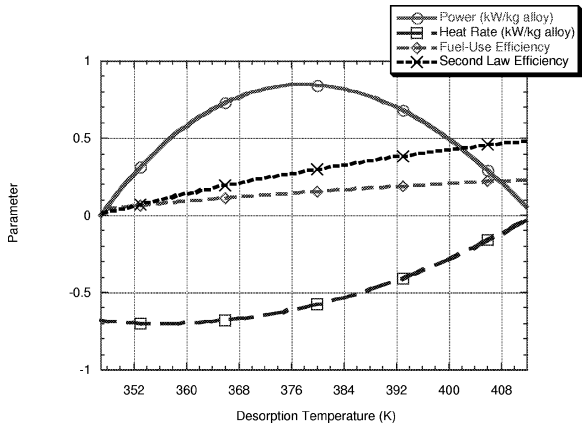

Figure 7. Heating mode performance as a function of desorption temperature.

TABLE II
System parameters used to construct power and efficiency diagrams.

Mass of alloy	1 kg $LaNi_5$
Heat source temperature	413 K
Ambient temperature (heating mode)	281 K
Ambient temperature (cooling mode)	298 K
Cooled space temperature	281 K
Heated space temperature	298 K
Overall heat transfer coefficient	1.0 $kW{\cdot}m^{-2}{\cdot}K^{-1}$

The presence of maxima in the power and heat rate curves are a consequence of the following phenomenon as described by Curzon and Ahlborn [14]. In the absence of a temperature difference between a heat reservoir and the working fluid, the process of transferring heat would take an infinite amount of time and, hence, produce no power. Conversely, if the process occurs at an infinitely fast rate the temperature of the working fluid will not change and, again, no power will be produced. At some place in between these extremes exists a temperature difference which will result in the maximum rate of energy transfer for the given process.

Figures 6 and *7* show a maximum in the power curve for both heating and cooling modes, a maximum cooling rate and minimum heating rate (by convention, heat out of the cycle is taken to have a negative sign). The power and heat or cold rate approaches zero as the desorption temperature approaches the heat source temperature ($\Delta T \rightarrow 0$), as expected. However, the power also approaches zero as the desorption temperature approaches the absorption temperature; this is the situation on the far left hand side of each figure. At this point, the pressure ratio across the turbine is solely a function of the difference between pressures at the high and low concentration ends of the plateau. Since the plateau is quite flat for $LaNi_5$ this pressure difference is minimal and, hence, almost no power is produced. Decreases in desorption temperature below the absorption temperature are not meaningful physically. Nonetheless, even with a negligible power output at this point the gas can accept or reject heat, giving rise to the non-zero cold and heat rates evident in *figures 6* and *7*, respectively.

6. SYSTEM COMPARISONS

The power and heat rates and the first and second law efficiencies of the present cycle will now be compared to HYCSOS and the system developed by Bomin Solar. The HYCSOS system used pairs of $LaNi_5$ and $CaNi_5$ beds [13, 15, 16]. The Bomin Solar system was made using Mg doped with a small amount of Ni in order to eliminate the hazard of pyrophoricity [6, 17].

Tables III and *IV* provide comparable information for the HYCSOS and Bomin Solar systems, respectively. The HYCSOS system is described as being operable in one of three modes: heating, refrigeration and energy conversion [13]. The energy conversion mode is described as being suitable when both power and space heating are desired. However, listed efficiencies are based on the data given for power generation only. The data presented for

TABLE III
Design and operational parameters for HYCSOS in energy conversion mode (power) and refrigeration mode.

Mass of alloy	13.6 kg $LaNi_5$
Heat source temperature	413 K
Ambient temperature	298 K (power) 313 K (refrigeration)
Cooled space temperature	281 K
Cycle time	4 min
Power generated	0.06 $kW \cdot kg^{-1}$ alloy
Useful cold rate	0.30 $kW \cdot kg^{-1}$ alloy
First law efficiency	0.165 (power)
Second law efficiency	0.60 (power)

TABLE IV
Design and operational parameters for Bomin Solar system.

Mass of alloy	20 kg Mg
Heat source temperature	753 K
Heat sink temperature	333 K
Heated space temperature	353 K
Cycle time	120 min
Power generated	0.05 $kW \cdot kg^{-1}$ alloy
Useful heat rate	0.30 $kW \cdot kg^{-1}$ alloy
Fuel-use efficiency	0.11
Second law efficiency	0.543

the Bomin Solar system is for generation of power and useful heat, but Groll et al. [17] claim the system can generate useful cold as well as heat and power simultaneously. The value of the heat sink temperature used was that of the Stirling engine cooling water.

The thermal efficiency of the present cycle in heating mode based solely on its power output would be 0.13, slightly lower than the HYCSOS value. The second law efficiency calculated on this basis for the present cycle would be 0.24, significantly less than the HYCSOS value. The power generated by the present cycle per kg of alloy is nearly twice that of the HYCSOS system, however.

One additional comment on HYCSOS is that the second law analysis presented here does indicate that lower absorption temperatures will result in greater efficiency as noted by Gruen et al. [5]. However, those authors also indicate that to provide space heating in addition to power the absorption process could be operated at a higher temperature, say 323 K. This method of providing heating will introduce large external irreversibilities into the cycle which may be reduced by using a heat exchanger with a smaller ΔT.

The Bomin Solar system, if operated at an ambient temperature of 298 K, is substantially less efficient (from either a first or second law perspective) than the present cycle and generates less power per kg of alloy. However, the Bomin Solar system generates more than four times as much useful heat as the present cycle.

7. CONCLUSIONS

A first and second law analysis has been presented for a heat-driven metal hydride cogeneration cycle. Second law analysis places bounds on the temperatures of the heat source and sink reservoirs the cycle may communicate with. In addition, a finite-time analysis provides expressions for the power and heat rates of the cycle in terms of design and operating parameters.

The foregoing analysis assumed no pressure drops in the heat exchangers, ideal gas behavior, spatial uniformity of temperature and pressure in the hydride beds and heat transfer as the rate-limiting step for ab/desorption. Nevertheless, practical lessons may be drawn from this idealized analysis. The constraints on operating temperatures suggested by first and second law analysis are helpful in selecting both appropriate applications and hydridable alloys for those applications. For all cycles considered the qualitative benefits of one over the other in terms of first or second law efficiency (expected based on the present analysis) must be weighed against the difference in cost between their respective components, including the hydridable alloy chosen. The maxima in power and heat/cold rates suggested by the finite-time analysis can also be used as qualitative considerations in designing hardware since they may be used to estimate required coolant mass flow rates and heat exchanger areas for a proposed application.

Within the limitations of this analysis the present cycle offers superior levels of power generation and first law efficiency, while the HYCSOS system will offer superior second law efficiencies. The HYCSOS and Bomin Solar systems appear equally best suited for space heating and cooling. Hydride power and heat transforming cycles have been proposed for more than 25 years as alternatives to conventional fossil fuel systems. Recently it has been proposed [6] that small-scale hydride systems may be competitive in “regions without a public grid” or “rural small communities”. A cost analysis performed on the HYCSOS system developed at Argonne National Laboratory [16] did not indicate that significant economic advantages existed at that time. Future work will revisit that question.

REFERENCES

[1] Wolf S., Hydrogen sponge heat pump, in: Proceedings of the 10th Intersociety Energy Conversion Engineering Conference (IECEC), 1975, Paper 759196, pp. 1348–1351.

[2] McClaine A.W., Method and apparatus for heat transfer, using metal hydrides, US Patent 4,039,023, 1977.

[3] Terry L.E., Schoeppel R.J., Hydride–dehydride power system and methods, US Patent 3,943,719, 1976.

[4] Powell J.R., Salzano F.J., Wen-Shi Y., Milau J.S., High efficiency power conversion cycles using hydrogen compressed by absorption on metal hydrides, in: Proceedings of the 10th Intersociety Energy Conversion Engineering Conference (IECEC), 1975, pp. 1339–1347.

[5] Gruen D.M., Schreiner F., Sheft I., A thermodynamic analysis of HYCSOS, a hydrogen conversion and storage system, Int. J. Hydrogen Energy 3 (3) (1978) 303–310.

[6] Wierse M., Werner R., Groll M., Magnesium hydride for thermal energy storage in a small-scale solar-thermal power station, J. Less-Common Metals 172–174 (1991) 1111–1121.

[7] Ikeda N., Tani T., Tanaka T., Horigome T., Conceptual design of solar thermal power system with metallic hydride, in: Solar Thermal Central Receiver Systems: Proceedings of the Third International Workshop, Vol. 2, 1986, pp. 929–942.

[8] Kim K.J., Feldman K.T., Jr., Lloyd G., Razani A., Compressor-driven heat pump development employing porous metal hydride compacts, ASHRAE Trans. 104 (1B) (1998) 1434–1445.

[9] Mueller W.M., Blackledge J.P., Libowitz G.G., Metal Hydrides, Academic Press, New York, 1968.

[10] Pons M., Dantzer P., Heat transfer in metal hydride packed beds. II: A new experimental technique and results on $LaNi_5$ powder, Z. Phys. Chem. 183 (1–2) (1994) 213–223.

[11] Huang F.F., A methodology for performance evaluation of combustion gas turbine cogeneration systems based on first law as well as second-law analysis, ASME HTD Vol. 97/AES, Vol. 6, 1988, pp. 35–40.

[12] Wu C., Kiang R.L., Finite-time thermodynamic analysis of a Carnot engine with internal irreversibility, Energy 17 (12) (1992) 1173–1178.

[13] Gruen D.M., Sheft I., Lamich G., Mendelsohn M., HYCSOS: A chemical heat pump and energy conversion system based on metal hydrides, Argonne National Laboratory Report ANL-77-39, 1977.

[14] Curzon F.L., Ahlborn B., Efficiency of a Carnot engine at maximum power output, Amer. J. Phys. 43 (1975) 22–24.

[15] Horowitz J.S., HYCSOS: Hydride conversion and storage system sensitivity analysis, Argonne National Laboratory Report ANL/EES-TM-63, 1979.

[16] Gorman R., Performance and cost analysis of a hydride air conditioning system, Argonne National Laboratory Report ANL/EES-TM-65, 1977.

[17] Groll M., Isselhorst A., Wierse M., Metal hydride devices for environmentally clean energy technology, Int. J. Hydrogen Energy 19 (6) (1994) 507–515.